Relativistic calculations of dielectronic recombination rate coefficients for Be-like ions

Mau Hsiung Chen
High Temperature Physics Division, Lawrence Livermore National Laboratory, University of California, Livermore, California 94550

Bernd Crasemann
Department of Physics and Chemical Physics Institute, University of Oregon, Eugene, Oregon 97403

(Received 6 June 1988)

The dielectronic recombination rate coefficients for the ten initial states of the $1s^2 2l 2l'$ configurations of the Be-like ions have been calculated for six ions with atomic numbers $Z=30$, 34, 36, 42, 47, and 54 in the isolated-resonance approximation. The detailed Auger and radiative rates for each autoionizing state were evaluated using the multiconfiguration Dirac-Fock model in intermediate coupling with configuration interaction. The present results are compared with the existing theoretical values and the predictions of the Burgess and the Burgess-Merts semiempirical formulas.

I. INTRODUCTION

Dielectronic recombination (DR) is a very important recombination process in high-temperature laboratory or astrophysical plasmas.[1,2] The dielectronic recombination process can affect the ionization balance[3] and the level population of a plasma.[4] In the early work of plasma modeling, the DR process was often taken into account by using rate coefficients computed from semiempirical formulas.[2,5] Recently, many distorted-wave calculations have been performed to determine the DR rate coefficients. For Be-like ions, the DR rate coefficients have been calculated for a few ions using nonrelativistic single-configuration Hartree-Fock wave functions in *LS* coupling and in an angular-momentum-averaged scheme.[6-8]

In this paper we report on calculations of dielectronic recombination rate coefficients for the ten initial states of Be-like ions with $1s^2 2l 2l'$ configurations. The calculations cover six ions with atomic numbers $Z=30$, 34, 36, 42, 47, and 54. The detailed Auger and radiative rates for each autoionizing states were calculated using the multiconfiguration Dirac-Fock model[9-11] (MCDF) in intermediate coupling with configuration interaction within the same complex. The DR rate coefficients from the present MCDF calculations are compared with previous theoretical values from nonrelativistic Hartree-Fock calculations and predictions from the semiempirical Burgess[2] and Burgess-Merts formulas.[5]

II. THEORETICAL CALCULATIONS

The dielectronic recombination coefficients from an initial site i of the recombining ion to a stabilized final state f via an intermediate autoionizing state d can be expressed as

$$\alpha_{\mathrm{DR}}(idf)=\frac{1}{2g_i}\left[\frac{4\pi R}{kT}\right]^{3/2} a_0^3 \exp(-e_2/kT) \times g_d A_a(d\rightarrow i)\omega_d \ , \tag{1}$$

where

$$\omega_d = A_r(d\rightarrow f)/[\Gamma_r(d)+\Gamma_a(d)] \ . \tag{2}$$

Here g_d and g_i are the statistical weight factors; R is the Rydberg energy and a_0 is the Bohr radius; $A_a(d\rightarrow i)$ is the Auger rate and $A_r(d\rightarrow f)$ is the radiative rate; e_2 is the Auger energy and T is the plasma electron temperature; $\Gamma_r(d)$ and $\Gamma_a(d)$ are the total radiative and Auger rates for the autoionizing state d, respectively. The Auger and radiative rates are in sec^{-1} and DR rate coefficients are in units of $\mathrm{cm}^3/\mathrm{sec}$. The total dielectronic recombination rate coefficient can be obtained from Eq. (1) by summing over d and f. In the derivation of Eq. (1), we use the isolated-resonance approximation and assume a Maxwellian distribution of the plasma electrons.

The detailed Auger and radiative rates and transition energies required for the evaluation of Eqs. (1) and (2) were calculated explicitly for each autoionizing state. The Auger transition probability in a frozen-orbital approximation is given in perturbation theory by[9,12]

$$A_a(d\rightarrow i)=\frac{2\pi}{\hbar}\left|\left\langle \Psi_i \left| \sum_{\substack{\alpha,\beta \\ (\alpha<\beta)}} \frac{e^2}{r_{\alpha\beta}} \right| \Psi_d \right\rangle\right|^2 \rho(\epsilon) \ , \tag{3}$$

where $\rho(\varepsilon)$ is the density of final states.

For spontaneous electric-dipole radiative transitions, the probability for a discrete transition $d\rightarrow f$ is calculated from perturbation theory[9,13] as

$$A_r(d\rightarrow f)=\frac{2\pi}{3(2J_d+1)}|\langle f\|T_1\|d\rangle|^2 \ , \tag{4}$$

where $\langle f\|T_1\|d\rangle$ is the electric-dipole reduced matrix element.[13]

In the present work, the Auger and radiative matrix elements in Eqs. (3) and (4) were evaluated in the framework of the MCDF model. Details are described in Ref. 9.

Dielectric recombination from a state of a Be-like ion with a $1s^2 2l 2l'$ configuration can occur through $\Delta n \neq 0$

and $\Delta n=0$ transitions. For the $\Delta n\neq 0$ transitions involving excitation from the $n=2$ subshell, the DR process can be represented by

$$1s^2 2l_1 2l_2 + e \rightleftarrows 1s^2 2l_3 nln'l' \rightarrow 1s^2 2l_3 2l_4 n''l'' + h\nu \ . \quad (5)$$

We also performed sample calculations to investigate the contributions to the total DR coefficients from K-shell excitation.

For the $\Delta n=0$ transitions, the following processes were included in the present work:

$$1s^2 2s^2 + e \rightleftarrows 1s^2 2s 2pnl \rightarrow (1s^2 2s^2 nl + 1s^2 2s 2pn'l') + h\nu \ , \quad (6)$$

$$1s^2 2s 2p + e \rightleftarrows 1s^2 2p^2 nl \rightarrow (1s^2 2s 2pnl + 1s^2 2p^2 n'l') + h\nu \ , \quad (7)$$

$$1s^2 2p_{1/2}^2 + e \rightleftarrows 1s^2 2p_{1/2} 2p_{3/2} nl \rightarrow (1s^2 2s 2p_{3/2} nl + 1s^2 2s 2p_{1/2} nl + 1s^2 2p_{1/2} 2p_{3/2} n'l') + h\nu \ , \quad (8)$$

and

$$1s^2 2p_{1/2} 2p_{3/2} + e \rightleftarrows 1s^2 2p_{3/2}^2 nl \rightarrow (1s^2 2s 2p_{3/2} nl + 1s^2 2p_{3/2}^2 n'l') + h\nu \ . \quad (9)$$

For the $\Delta n\neq 0$ transitions [Eq. (5)], explicit calculations were carried out for the intermediate states with $n=3$ and $n'\leq 10$ and $l'\leq 5$. For the $\Delta n=0$ transitions [Eqs. (6)–(9)], we included detailed calculations for $n\leq 30$ and $l\leq 8$. The contributions from the autoionizing levels with $10<n'\leq 30$ for the $\Delta n\neq 0$ transitions and $30<n\leq 200$ for the $\Delta n=0$ transitions were taken into account by using an n^{-3} extrapolation of the transition rates. In the calculations of the fluorescence yield ω_d [Eq. (2)], we included all possible Auger channels and the electric dipole-allowed radiative transitions from inner as well as Rydberg electrons. The radiative transitions leading to other autoionizing states, however, were neglected in the present calculations.

The atomic energy levels and bound-state wave functions needed in the present work were calculated according to the MCDF model in the average-level scheme.[11] The calculations were performed in intermediate coupling with configuration interaction from the same complex. The continuum wave functions required in calculations of the Auger matrix elements were obtained by solving the Dirac-Fock equations for the final state without including the exchange interaction between the bound and continuum electrons. The term-dependent Auger and radiative rates were computed according to Eqs. (3) and (4), respectively. These atomic transition rates were then used to calculate the DR rate coefficients [Eqs. (1) and (2)].

III. RESULTS AND DISCUSSION

The total DR coefficients for the ten initial states from the $1s^2 2l 2l'$ configurations of the Be-like ions have been calculated for six ions with atomic numbers $30\leq Z\leq 54$ for electron temperatures $0.01\leq T\leq 20$ keV. The calculations were carried out using the MCDF method including intermediate coupling and configuration interaction

TABLE I. Calculated dielectronic recombination rate coefficients (in cm^3/sec) for the Be-like $_{30}Zn^{26+}$ ion. Numbers in square brackets signify powers of ten. Values listed in the first and second rows for each initial state are rates for the $\Delta n\neq 0$ and $\Delta n=0$ transitions, respectively. The notation $(2p_{1/2}2p_{3/2})_1$ indicates $2p_{1/2}2p_{3/2}J=1$ state. The $1s^2$ core is omitted in this designation.

Initial state	Temperature (keV) 0.05	0.10	0.40	1.0	2.0	3.0	4.0
$(2s^2)_0$	3.62[−14]	1.30[−12]	1.04[−11]	1.05[−11]	6.34[−12]	4.17[−12]	2.97[−12]
	1.23[−10]	6.57[−11]	1.22[−11]	3.38[−12]	1.23[−12]	6.79[−13]	4.43[−13]
$(2s2p_{1/2})_0$	9.96[−14]	2.69[−12]	1.71[−11]	1.60[−11]	9.47[−12]	6.16[−12]	4.37[−12]
	5.05[−11]	2.60[−11]	4.62[−11]	1.27[−12]	4.60[−13]	2.52[−13]	1.65[−13]
$(2s2p_{1/2})_1$	9.48[−14]	2.52[−12]	1.65[−11]	1.59[−11]	9.41[−12]	6.13[−12]	4.36[−12]
	5.10[−11]	2.68[−11]	4.78[−12]	1.31[−12]	4.75[−13]	2.61[−13]	1.70[−13]
$(2s2p_{3/2})_2$	1.30[−13]	2.93[−12]	1.69[−11]	1.58[−11]	9.24[−12]	5.99[−12]	4.26[−12]
	4.97[−11]	2.64[−11]	4.74[−12]	1.29[−12]	4.72[−13]	2.59[−13]	1.69[−13]
$(2s2p_{3/2})_1$	2.15[−13]	3.68[−12]	1.76[−11]	1.60[−11]	9.33[−12]	6.04[−12]	4.28[−12]
	5.91[−11]	3.02[−11]	5.18[−12]	1.40[−12]	5.08[−13]	2.78[−13]	1.82[−13]
$(2p^2_{1/2})_0$	2.67[−13]	4.88[−12]	2.25[−11]	1.96[−11]	1.12[−11]	7.24[−12]	5.13[−12]
	8.05[−12]	3.18[−12]	4.34[−13]	1.12[−13]			
$(2P_{1/2}2p_{3/2})_1$	3.40[−13]	5.63[−12]	2.54[−11]	2.20[−11]	1.26[−11]	8.14[−12]	5.76[−12]
	4.11[−12]	1.73[−12]	2.48[−13]				
$(2p_{1/2}2p_{3/2})_2$	3.34[−13]	5.53[−12]	2.47[−11]	2.15[−11]	1.23[−11]	7.91[−12]	5.60[−12]
	3.25[−12]	1.35[−12]	1.92[−13]				
$(2p^2_{3/2})_2$	4.04[−13]	6.08[−12]	2.50[−11]	2.16[−11]	1.24[−11]	7.97[−12]	5.63[−12]
$(2p^2_{3/2})_0$	5.71[−13]	6.48[−12]	2.31[−11]	1.98[−11]	1.13[−11]	7.27[−12]	5.13[−12]

TABLE II. Calculated dielectronic recombination rate coefficients (in cm^3/sec) for the Be-like $_{34}Se^{30+}$ ion. The rates listed in first and second rows for each initial state are the values for the $\Delta n \neq 0$ and $\Delta n = 0$ transitions, respectively. Numbers in square brackets signify powers of ten.

Initial state	Temperature (keV) 0.05	0.10	0.40	1.0	2.0	3.0	4.0
$(2s^2)_0$	4.15[−15]	4.96[−13]	8.26[−12]	1.02[−11]	6.97[−12]	4.78[−12]	3.49[−12]
	2.24[−10]	1.19[−10]	2.29[−11]	6.40[−12]	2.35[−12]	1.29[−12]	8.43[−13]
$(2s2p_{1/2})_0$	1.23[−14]	1.12[−12]	1.41[−11]	1.58[−11]	1.03[−11]	7.00[−12]	5.08[−12]
	7.11[−11]	3.91[−11]	7.60[−12]	2.13[−12]	7.79[−13]	4.29[−13]	2.80[−13]
$(2s2p_{1/2})_1$	1.34[−14]	1.15[−12]	1.42[−11]	1.59[−11]	1.04[−11]	7.04[−12]	5.12[−12]
	7.73[−11]	4.18[−11]	7.87[−12]	2.18[−12]	7.98[−13]	4.40[−13]	2.87[−13]
$(2s2p_{3/2})_2$	2.52[−14]	1.52[−12]	1.49[−11]	1.60[−11]	1.04[−11]	7.01[−12]	5.08[−12]
	6.68[−11]	3.67[−11]	7.06[−12]	1.97[−12]	7.20[−13]	3.96[−13]	2.58[−13]
$(2s2p_{3/2})_1$	4.10[−14]	1.88[−12]	1.52[−11]	1.61[−11]	1.04[−11]	7.02[−12]	5.09[−12]
	7.30[−11]	4.16[−11]	8.01[−12]	2.23[−12]	8.13[−13]	4.47[−13]	2.92[−13]
$(2p_{1/2}^2)_0$	4.25[−14]	2.33[−12]	2.01[−11]	1.98[−11]	1.25[−11]	8.35[−12]	6.04[−12]
	1.41[−11]	6.11[−12]	8.96[−13]	2.34[−13]			
$(2P_{1/2}2p_{3/2})_1$	6.19[−14]	2.90[−12]	2.28[−11]	2.24[−11]	1.40[−11]	9.35[−12]	6.75[−12]
	6.03[−12]	2.81[−12]	4.41[−13]	1.17[−13]			
$(2p_{1/2}2p_{3/2})_2$	6.34[−14]	2.92[−12]	2.25[−11]	2.20[−11]	1.38[−11]	9.20[−12]	6.64[−12]
	5.49[−12]	2.50[−12]	3.83[−13]	1.01[−13]			
$(2p_{3/2}^2)_2$	8.30[−14]	3.24[−12]	2.23[−11]	2.20[−11]	1.38[−11]	9.23[−12]	6.66[−12]
	2.95[−14]	1.16[−14]					
$(2P_{3/2}^2)_0$	1.28[−13]	3.78[−12]	2.14[−11]	2.09[−11]	1.31[−11]	8.72[−12]	6.29[−12]

from the same complex. The results for the $\Delta n \neq 0$ and $\Delta n = 0$ transitions are listed in Tables I–VI for some selected temperatures. The states are identified by their dominant *j-j* component.

For each autoionizing level we include all of the possible Auger decay channels and radiative channels leading to the stabilized bound states. The radiative transitions to the other autoionizing states were neglected both in A_r and Γ_r of Eq. (2). This radiative cascade effect has been found to reduce the DR rate coefficient for the Mo^{38+} ion by only about 5%.[6,7]

In the present work the contributions from autoioniz-

TABLE III. Calculated dielectronic recombination rate coefficients (in cm^3/sec) for the Be-like $_{36}Kr^{32+}$ ion. The rate coefficients for the $\Delta n \neq 0$ and $\Delta n = 0$ transitions are listed in the first and second rows, respectively, for each initial state. Numbers in square brackets signify powers of ten.

Initial state	Temperature (keV) 0.05	0.10	0.40	1.0	2.0	3.0	4.0
$(2s^2)_0$	1.28[−15]	2.96[−13]	7.55[−12]	1.01[−11]	7.23[−12]	5.07[−12]	3.75[−12]
	1.80[−10]	1.01[−10]	2.12[−11]	6.05[−12]	2.23[−12]	1.23[−12]	8.03[−13]
$(2s2p_{1/2})_0$	3.68[−15]	6.57[−13]	1.28[−11]	1.53[−11]	1.06[−11]	7.32[−12]	5.37[−12]
	6.79[−11]	4.03[−11]	8.45[−12]	2.41[−12]	8.87[−13]	4.93[−13]	3.20[−13]
$(2s2p_{1/2})_1$	4.04[−15]	6.63[−13]	1.26[−11]	1.53[−11]	1.05[−11]	7.31[−12]	5.38[−12]
	8.66[−11]	4.83[−11]	9.46[−12]	2.65[−12]	9.71[−13]	5.35[−13]	3.49[−13]
$(2s2p_{3/2})_2$	9.20[−15]	9.64[−13]	1.36[−11]	1.57[−11]	1.07[−11]	7.41[−12]	5.44[−12]
	6.96[−11]	3.98[−11]	8.03[−12]	2.27[−12]	8.31[−13]	4.59[−13]	3.00[−13]
$(2s2p_{3/2})_1$	1.62[−14]	1.27[−12]	1.44[−11]	1.62[−11]	1.10[−11]	7.55[−12]	5.53[−12]
	7.70[−11]	4.61[−11]	9.41[−12]	2.65[−12]	9.74[−13]	5.37[−13]	3.51[−13]
$(2p_{1/2}^2)_0$	1.45[−14]	1.45[−12]	1.88[−11]	1.99[−11]	1.32[−11]	8.99[−12]	6.56[−12]
	1.82[−11]	8.33[−12]	1.28[−12]	3.38[−13]	1.21[−13]		
$(2p_{1/2}2p_{3/2})_1$	2.32[−14]	1.84[−12]	2.09[−11]	2.18[−11]	1.43[−11]	9.74[−12]	7.10[−12]
	8.56[−12]	4.11[−12]	6.67[−13]	1.78[−13]			
$(2p_{1/2}2p_{3/2})_2$	2.37[−14]	1.87[−12]	2.08[−11]	2.15[−11]	1.41[−11]	9.64[−12]	7.02[−12]
	6.32[−12]	3.09[−12]	5.02[−13]	1.34[−13]			
$(2p_{3/2}^2)_2$	3.22[−14]	2.13[−12]	2.05[−11]	2.16[−11]	1.42[−11]	9.70[−12]	7.07[−12]
	2.18[−14]						
$(2p_{3/2}^2)_0$	5.47[−14]	2.64[−12]	2.06[−11]	2.10[−11]	1.37[−11]	9.34[−12]	6.80[−12]

TABLE IV. Calculated dielectronic recombination rate coefficients (in cm^3/sec) for the Be-like $_{42}Mo^{38+}$ ion. The results for the $\Delta n \neq 0$ and $\Delta n = 0$ transitions are listed in the first and second rows, respectively, for each initial state. Numbers in square brackets signify powers of ten.

Initial state	Temperature (keV) 0.05	0.10	0.40	1.0	2.0	3.0	4.0	5.0
$(2s^2)_0$		3.90[−14]	5.03[−12]	8.54[−12]	7.21[−12]	5.44[−12]	4.18[−12]	3.32[−12]
	1.96[−10]	1.21[−10]	3.05[−11]	9.22[−12]	3.48[−12]	1.93[−12]	1.27[−12]	9.14[−13]
$(2s2p_{1/2})_0$		8.48[−14]	8.48[−12]	1.29[−11]	1.03[−11]	7.65[−12]	5.83[−12]	4.60[−12]
	1.30[−10]	7.33[−11]	1.67[−11]	4.95[−12]	1.85[−12]	1.03[−12]	6.73[−13]	4.85[−13]
$(2s2p_{1/2})_1$		8.86[−14]	8.23[−12]	1.27[−11]	1.03[−11]	7.62[−12]	5.82[−12]	4.60[−12]
	1.21[−10]	7.28[−11]	1.66[−11]	4.88[−12]	1.82[−12]	1.01[−12]	6.59[−13]	4.74[−13]
$(2s2p_{3/2})_2$		1.94[−13]	9.82[−12]	1.36[−11]	1.06[−11]	7.79[−12]	5.92[−12]	4.66[−12]
	8.81[−11]	5.42[−11]	1.26[−11]	3.73[−12]	1.39[−12]	7.71[−13]	5.06[−13]	3.63[−13]
$(2s2p_{3/2})_1$		2.90[−13]	1.13[−11]	1.46[−11]	1.12[−11]	8.18[−12]	6.19[−12]	4.87[−12]
	1.03[−10]	6.68[−11]	1.65[−11]	4.92[−12]	1.84[−12]	1.02[−12]	6.70[−13]	4.82[−13]
$(2p_{1/2}^2)_0$		2.08[−13]	1.25[−11]	1.69[−11]	1.31[−11]	9.56[−12]	7.24[−12]	5.70[−12]
	3.97[−11]	1.98[−11]	3.43[−12]	9.31[−13]	3.37[−13]	1.85[−13]	1.21[−13]	8.65[−14]
$(2p_{1/2}2p_{3/2})_1$		3.41[−13]	1.47[−11]	1.89[−11]	1.42[−11]	1.03[−11]	7.80[−12]	6.13[−12]
	1.01[−11]	6.10[−12]	1.24[−12]	3.48[−13]	1.27[−13]			
$(2p_{1/2}2p_{3/2})_2$		3.56[−13]	1.48[−11]	1.87[−11]	1.40[−11]	1.02[−11]	7.67[−12]	6.02[−12]
	1.07[−11]	6.04[−12]	1.16[−12]	3.22[−13]	1.18[−13]			
$(2p_{3/2}^2)_2$		5.15[−13]	1.64[−11]	1.97[−11]	1.47[−11]	1.06[−11]	7.96[−12]	6.24[−12]
$(2p_{3/2}^2)_0$		7.27[−13]	1.75[−11]	2.02[−11]	1.47[−11]	1.06[−11]	7.95[−12]	6.22[−12]

TABLE V. Calculated dielectronic recombination rate coefficients (in cm^3/sec) for the Be-like $_{47}Ag^{43+}$ ion. The contributions from the $\Delta n \neq 0$ and $\Delta n = 0$ transitions are listed in the first and second rows, respectively, for each initial state. Numbers in square brackets signify powers of ten.

Initial state	Temperature (keV) 0.05	0.10	0.40	1.0	2.0	3.0	4.0	5.0
$(2s^2)_0$		4.91[−15]	3.42[−12]	7.26[−12]	6.88[−12]	5.50[−12]	4.37[−12]	3.53[−12]
	1.75[−10]	1.23[−10]	3.88[−11]	1.27[−11]	4.90[−12]	2.75[−12]	1.81[−12]	1.31[−12]
$(2s2p_{1/2})_0$		9.27[−15]	5.18[−12]	1.03[−11]	9.35[−12]	7.35[−12]	5.79[−12]	4.68[−12]
	9.50[−11]	6.79[−11]	2.09[−11]	6.73[−12]	2.59[−12]	1.45[−12]	9.57[−13]	6.91[−13]
$(2s2p_{1/2})_1$		1.07[−14]	5.26[−12]	1.03[−11]	9.45[−12]	7.44[−12]	5.88[−12]	4.74[−12]
	1.28[−10]	8.45[−11]	2.31[−11]	7.20[−12]	2.74[−12]	1.53[−12]	1.01[−12]	7.26[−13]
$(2s2p_{3/2})_2$		4.05[−14]	7.13[−12]	1.17[−11]	1.01[−11]	7.81[−12]	6.11[−12]	4.90[−12]
	9.09[−11]	6.21[−11]	1.68[−11]	5.23[−12]	1.99[−12]	1.11[−12]	7.32[−13]	5.28[−13]
$(2s2p_{3/2})_1$		6.63[−14]	8.50[−12]	1.29[−11]	1.08[−11]	8.29[−12]	6.46[−12]	5.17[−12]
	1.08[−10]	7.64[−11]	2.30[−11]	7.33[−12]	2.81[−12]	1.57[−12]	1.04[−12]	7.48[−13]
$(2p_{1/2}^2)_0$		2.56[−14]	8.35[−12]	1.44[−11]	1.24[−11]	9.57[−12]	7.47[−12]	5.99[−12]
	4.96[−11]	2.96[−11]	6.33[−12]	1.81[−12]	6.69[−13]	3.70[−13]	2.41[−13]	1.74[−13]
$(2p_{1/2}2p_{3/2})_1$		7.41[−14]	1.07[−11]	1.65[−11]	1.37[−11]	1.04[−11]	8.07[−12]	6.45[−12]
	1.41[−11]	8.87[−12]	2.15[−12]	6.38[−13]	2.39[−13]	1.32[−13]	8.67[−14]	6.24[−14]
$(2p_{1/2}2p_{3/2})_2$		7.55[−14]	1.07[−11]	1.62[−11]	1.34[−11]	1.02[−11]	7.92[−12]	6.33[−12]
	9.92[−12]	7.11[−12]	1.80[−12]	5.34[−13]	2.00[−13]	1.11[−13]	7.25[−14]	5.22[−14]
$(2p_{3/2}^2)_2$		1.20[−13]	1.26[−11]	1.76[−11]	1.42[−11]	1.07[−11]	8.29[−12]	6.60[−12]
$(2p_{3/2}^2)_0$		1.70[−13]	1.35[−11]	1.80[−11]	1.44[−11]	1.08[−11]	8.34[−12]	6.63[−12]

TABLE VI. Calculated dielectronic recombination rate coefficients (in cm^3/sec) for the Be-like $_{54}Xe^{50+}$ ion. The contributions from the $\Delta n \neq 0$ and $\Delta n = 0$ transitions are listed in the first and second rows, respectively, for each initial state. Numbers in square brackets signify powers of ten.

Initial state	Temperature (keV) 0.05	0.10	0.40	1.0	2.0	3.0	4.0	5.0
$(2s^2)_0$			1.44[−12]	4.95[−12]	5.62[−12]	4.89[−12]	4.10[−12]	3.44[−12]
	8.90[−11]	8.64[−11]	4.47[−11]	1.72[−11]	7.07[−12]	4.05[−12]	2.71[−12]	1.96[−12]
$(2s2p_{1/2})_0$			2.20[−12]	6.99[−12]	7.55[−12]	6.45[−12]	5.34[−12]	4.45[−12]
	1.56[−10]	8.84[−11]	3.05[−11]	1.09[−11]	4.41[−12]	2.51[−12]	1.67[−12]	1.21[−12]
$(2s2p_{1/2})_1$			2.27[−12]	7.09[−12]	7.66[−12]	6.56[−12]	5.44[−12]	4.53[−12]
	1.23[−10]	8.15[−11]	3.05[−11]	1.08[−11]	4.35[−12]	2.48[−12]	1.64[−12]	1.19[−12]
$(2s2p_{3/2})_2$			4.13[−12]	9.11[−12]	8.86[−12]	7.31[−12]	5.95[−12]	4.92[−12]
	1.40[−10]	8.46[−11]	2.40[−11]	8.03[−12]	3.16[−12]	1.79[−12]	1.18[−12]	8.55[−13]
$(2s2p_{3/2})_1$			4.91[−12]	9.99[−12]	9.43[−12]	7.73[−12]	6.27[−12]	5.17[−12]
	1.06[−10]	8.13[−11]	3.18[−11]	1.15[−11]	4.62[−12]	2.63[−12]	1.75[−12]	1.27[−12]
$(2p_{1/2}^2)_0$			3.65[−12]	1.01[−11]	1.03[−11]	8.57[−12]	7.02[−12]	5.81[−12]
	3.43[−11]	2.81[−11]	9.43[−12]	3.05[−12]	1.18[−12]	6.60[−13]	4.35[−13]	3.14[−13]
$(2p_{1/2}2p_{3/2})_1$			5.90[−12]	1.26[−11]	1.18[−11]	9.66[−12]	7.81[−12]	6.41[−12]
	8.45[−12]	7.45[−12]	2.90[−12]	9.86[−13]	3.87[−13]	2.18[−13]	1.44[−13]	1.04[−13]
$(2p_{1/2}2p_{3/2})_2$			5.86[−12]	1.23[−11]	1.15[−11]	9.41[−12]	7.61[−12]	6.25[−12]
	8.05[−12]	6.82[−12]	2.59[−12]	8.75[−13]	3.42[−13]	1.93[−13]	1.27[−13]	9.20[−14]
$(2p_{3/2}^2)_2$		1.38[−14]	7.90[−12]	1.43[−11]	1.28[−11]	1.02[−11]	8.18[−12]	6.68[−12]
$(2p_{3/2}^2)_0$		2.22[−14]	8.84[−12]	1.52[−11]	1.33[−11]	1.05[−11]	8.42[−12]	6.86[−12]

ing levels with $l' > 5$ for the $\Delta n \neq 0$ transition [Eq. (5)] and $l > 8$ for the $\Delta n = 0$ transition [Eqs. (6)–(9)] were neglected. The contributions from $l' > 5$ for the $\Delta n \neq 0$ transition has been shown to be negligible for the He and Ne isoelectronic sequences.[10] The contribution to the DR rate coefficient from $8 \leq l \leq 15$ for the $\Delta n = 0$ transition is only a few percent for the fluorine isoelectronic sequence.[14]

In Fig. 1 the contributions to the DR rate coefficients from the intermediate $3lnl'$ configurations and the total DR rate coefficients from the $\Delta n \neq 0$ transitions for the $1s^2 2s^2 J = 0$ state of the Mo^{38+} ion are displayed. For electron temperatures $T \leq 3$ keV, the rate coefficients from $\Delta n \neq 0$ transitions are dominated by the contributions from the $3l3l'$ configurations. For higher temperatures, the contributions from high-n states become increasingly important (e.g., 30% of the total rate for $n \geq 7$ at $T = 10$ keV). For the purpose of comparison, the total DR rate for the $\Delta n \neq 0$ transitions from the nonrelativistic Hartree-Fock calculations[6,7] are also shown. The results from the present MCDF model deviate from the Hartree-Fock values by less than 20%. These differences could be partly due to the inclusion of relativistic effects in our present work.

The total DR rate coefficients for the $\Delta n \neq 0$ transitions for five different initial states of the Mo^{38+} ion are compared in Fig. 2. The DR rates from the initial $1s^2 2p^2$ states are larger than those for the initial $1s^2 2s 2p$ states by 35% while the rates for the $1s^2 2s 2p$ states are larger than the values for the $1s^2 2s^2$ state by 60% at the peak. This behavior is probably caused by the strong $2p$-$3d$ stabilizing radiative transition as opposed to the much

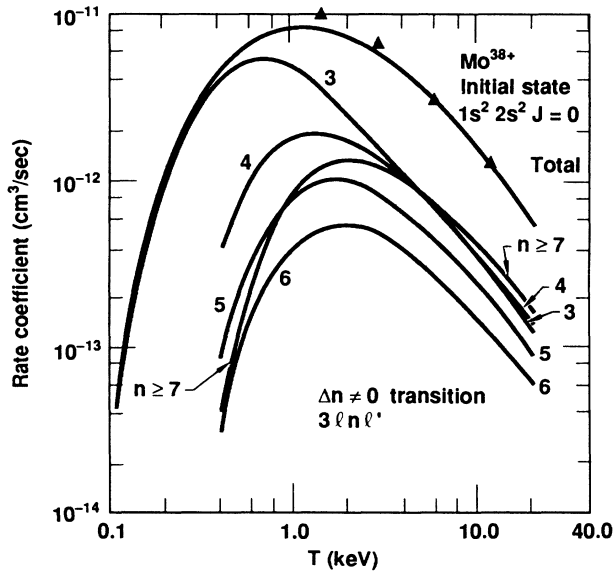

FIG. 1. Partial and total dielectronic recombination rate coefficients from $\Delta n \neq 0$ transitions for the initial $1s^2 2s^2 J = 0$ state of the Mo^{38+} ion as functions of electron temperature. The numbers on the curves are the principal quantum numbers n for the intermediate $3lnl'$ states. The solid triangles represent total DR rates for the $\Delta n \neq 0$ transitions from Ref. 7.

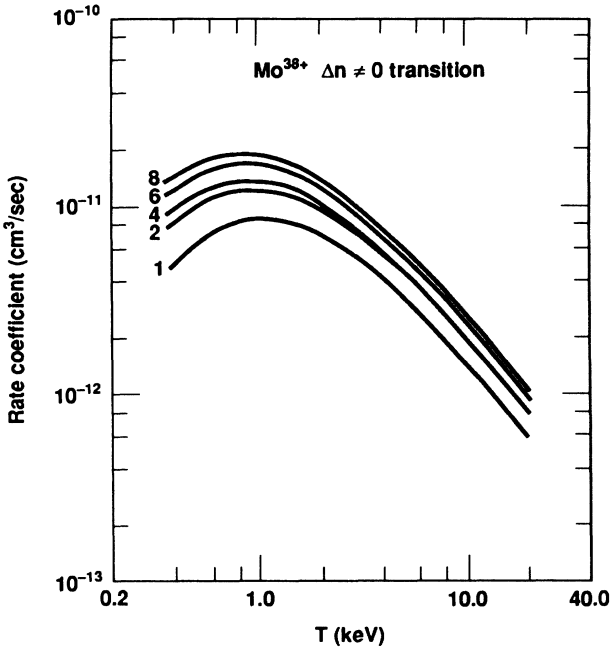

FIG. 2. Total DR rate coefficients from the $\Delta n \neq 0$ transitions for several initial states of the Mo^{38+} ion, as functions of temperature. The numbers on the curves are the initial levels in Table IV, ordered from the top.

weaker $2s$-$3p$ transition. In the low-temperature region, the differences in the DR rate coefficients for different fine-structure states can be as large as a factor of 2 (see Fig. 2 and Tables I–VI). The deviation diminishes as temperature increases.

In Fig. 3 the DR coefficients from the $\Delta n=0$ transitions for several initial states of the Mo^{38+} ion are displayed. For the initial $1s^22s^2$ and $1s^22s2p$ states, the dielectronic capture process can occur through the inverse Coster-Kronig $2s$-$2pnl$ transitions. The DR processes in the $\Delta n=0$ transitions for the $1s^22p_{1/2}2p_{3/2}$ states can proceed through the $2p_{1/2}$-$2p_{3/2}nl$ Coster-Kronig transitions which are made possible by the spin-orbit splitting of the $2p$ level. Since the onset of the $2p_{1/2}$-$2p_{3/2}nl$ Coster-Kronig transitions occurs at much higher n than that for the $2s$-$2pnl$ transitions, the DR rate coefficients from the $\Delta n=0$ transitions for the $1s^22p_{1/2}2p_{3/2}$ states are smaller than the corresponding values for the $1s^22s^2$ state by a factor of 4 to one order of magnitude (see Fig. 3). For electron temperatures $T \leq 0.1$ keV, the total DR coefficients are dominated by the $\Delta n=0$ transitions. As temperature increases, the contributions from the $\Delta n=0$ transitions to the total DR coefficients diminish quickly (e.g., 20% at $T=4$ keV for the $1s^22s^2$ state of the Mo^{38+} ion). Our present results for the $\Delta n=0$ transitions from the MCDF calculations for the $1s^22s^2$ state of the Mo^{38+} ion are larger than the values given by the nonrelativistic Hartree-Fock model by 15% (see Fig. 3).

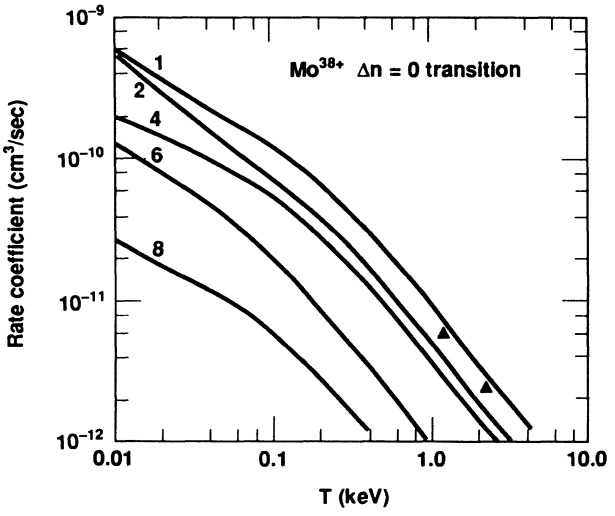

FIG. 3. DR rate coefficients from the $\Delta n=0$ transitions for the Mo^{38+} ion, as functions of temperature. The numbers on the curves are the initial levels listed in Table IV.

The present DR rate coefficients for the $1s^22s^2J=0$ state from the $\Delta n \neq 0$ transitions are compared with results from the semiempirical Burgess-Merts (BM) formula[5] in Fig. 4. For $T \leq 1$ keV, the MCDF results are larger than the BM predictions by as much as a factor of 6. On the other hand, the values from the semiempirical formula agree quite well with the MCDF results for higher temperatures. From Fig. 4, one can see the peak position shift from 0.7 to 2.6 keV and the peak rate reduced from 1.1×10^{-11} to 5.8×10^{-12} cm^3/sec as Z increases from 34 to 54.

In Fig. 5 the DR rate coefficients from our present work for the $1s^22s^2J=0$ state through the $\Delta n=0$ transitions are compared with predictions from the original Burgess semiempirical formula.[2] In applying the Burgess

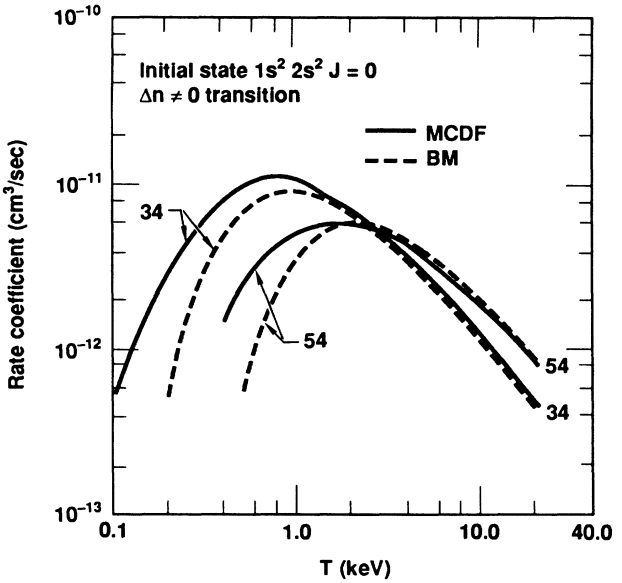

FIG. 4. Total DR rate coefficients from the $\Delta n \neq 0$ transitions for the initial $1s^22s^2J=0$ state, as functions of electron temperature. Solid curves indicate the present MCDF results. Dashed curves represent the values derived from the Burgess-Merts formula. Numbers on the curves are the atomic numbers.

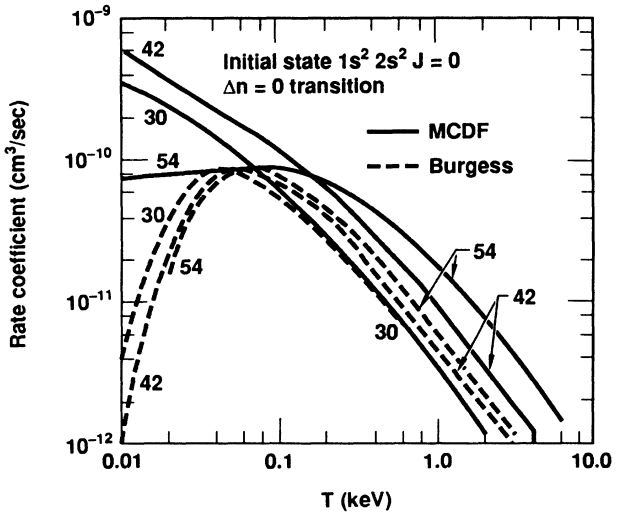

FIG. 5. DR rate coefficients from the $\Delta n=0$ transitions for the initial $1s^2 2s^2 J=0$ state as functions of electron temperature. Legends are the same as in Fig. 4.

formula, the required transition energies and oscillator strengths for the $\Delta n=0$ transitions were calculated from the fitted formula given in Ref. 15. At low temperatures, the DR rates from the Burgess formula are smaller than the results from the MCDF model by as much as one order of magnitude. For $T>50$ eV, the DR rates from the present MCDF calculations are larger than the results from the Burgess formula by a factor of 2, except for the Zn^{26+} ion.

In the present work we include contributions from L-shell excitation only. We have performed sample calculations to estimate the contributions from K-shell excitation. It was found that contributions from K-shell excitation to the total DR rate coefficients are negligibly small for $T \lesssim 4$ keV and are less than 5% for temperatures as high as 20 keV. Exclusion of K-shell contributions should therefore have very little impact on the total DR rate coefficients for electron temperatures under 20 keV. For much higher temperatures, the contributions from K-shell excitation should be included in calculations of the total DR rate coefficients.

ACKNOWLEDGMENTS

We gratefully acknowledge the expert computational efforts of Mei Chi Chen. We sincerely thank William F. Ballhaus, Jr., Director, NASA Ames Research Center (ARC), for permission to use the computational facilities of the Center, and thank the ARC Computational Chemistry and Aerothermodynamics branch, particularly David M. Cooper, for their hospitality. At the Lawrence Livermore National Laboratory, this work was performed in part under the auspices of the U.S. Department of Energy under Contract No. W-7405-ENG-48. In the University of Oregon, this research was supported in part by the National Science Foundation through Grant No. PHY-8516788 and by the Air Force Office of Scientific Research under Grant No. AFOSR-87-0026.

[1]M. J. Seaton and P. J. Storey, in *Atomic Processes and Applications,* edited by P. G. Burke and B. L. Moiseiwitsch (North-Holland, Amsterdam, 1976), p. 133.
[2]A. Burgess, Astrophys. J. **139**, 776 (1964); **141**, 1589 (1965).
[3]H. P. Summers, Mon. Not. R. Astron. Soc. **169**, 663 (1974).
[4]B. L. Whitten, A. U. Hazi, M. H. Chen, and P. L. Hagelstein, Phys. Rev. A **33**, 2171 (1986).
[5]A. L. Merts, R. D. Cowan, and N. H. Magee, Jr., Los Alamos Scientific Laboratory Report No. LA-6220-MS, 1976 (unpublished).
[6]J. N. Gau, Y. Hahn, and J. A. Retter, J. Quant. Spectrosc. Radiat. Transfer **23**, 131 (1980).
[7]Y. Hahn, J. N. Gau, R. Luddy, M. Dube, and N. Shkolnik, J. Quant. Spectrosc. Radiat. Transfer **24**, 505 (1980).
[8]K. LaGattuta and Y. Hahn, Phys. Rev. A **27**, 1675 (1983).
[9]M. H. Chen, Phys. Rev. A **31**, 1449 (1985).
[10]M.H. Chen, Phys. Rev. A **33**, 994 (1986); **34**, 1073 (1986).
[11]I. P. Grant, B. J. McKenzie, P. H. Norrington, D. F. Mayers, and N. C. Pyper, Comput. Phys. Commun. **21**, 207 (1980).
[12]W. Bambynek, B. Crasemann, R. W. Fink, H. U. Freund, H. Mark, C. D. Swift, R. E. Price, and P. V. Rao, Rev. Mod. Phys. **44**, 716 (1972).
[13]I. P. Grant, J. Phys. B **7**, 1458 (1974).
[14]L.J. Roszman (private communication).
[15]D. E. Post, R. V. Jensen, C. B. Tarter, W. H. Grasberger, and W. A. Lokke, At. Data Nucl. Data Tables **20**, 397 (1977).